Journal of Geophysical Research: Atmospheres

RESEARCH ARTICLE
10.1029/2018JD028962

Modeling Neutron Emissions in High Energy Atmospheric Phenomena

G. Diniz[1,2,3], C. Rutjes[3], U. Ebert[3,4], I. S. Ferreira[1], and E. F. M. T. São Sabbas[2]

[1]Instituto de Física, Universidade de Brasília, Brazil, [2]Instituto Nacional de Pesquisas Espaciais, Brazil, [3]Centrum Wiskunde & Informatica (CWI), Amsterdam, The Netherlands, [4]Department of Applied Physics, Eindhoven University of Technology, Eindhoven, The Netherlands

Key Points:
- We calculate neutron densities on ground for arbitrary spectra, altitudes, and durations of gamma-ray sources
- Neutron detection on ground indicates high gamma-ray energies at source altitude
- When the gamma-ray source is a directed beam, the effective neutron source is a cone of km length

Correspondence to:
G. Diniz,
gdiniz93@aluno.unb.br

Citation:
Diniz, G., Rutjes, C., Ebert, U., Ferreira, I. S., & São Sabbas, E. F. M. T. (2018). Modeling neutron emissions in high energy atmospheric phenomena. *Journal of Geophysical Research: Atmospheres*, *123*. https://doi.org/10.1029/2018JD028962

Received 7 MAY 2018
Accepted 25 OCT 2018
Accepted article online 1 NOV 2018

Abstract Neutron emissions with different durations have been observed during thunderstorms. These neutrons can be produced by microsecond to millisecond fast Terrestrial Gamma-ray Flashes correlated with lightning, or by Gamma-ray Glows lasting several seconds to minutes. In both cases, the neutrons are produced through a photonuclear reaction of gamma rays in the energy range of 10 to 30 MeV with nuclei of air molecules. Here we present simulations of gamma-ray beams propagating downward from different source altitudes. In our analysis the primary photons with energies between 10 and 30 MeV are separated into four energy intervals, each of 5 MeV width. From these data, arbitrary spectra of primary photons and of their products can be composed. Our results indicate that the neutrons are created essentially along the trajectory of the primary photons and that they reach ground within a transversal area of radius below 500 m. This lateral spreading is dominated by neutron diffusion due to collisions with air molecules. A secondary longer lasting photon pulse at sea level is predicted as well by our simulations. We have introduced this Terrestrial Gamma-ray Flash afterglow already in (Rutjes et al. 2017, https://doi.org/10.1002/2017GL075552). It is due to neutron capture by air molecules, and it has recently been observed by Bowers et al. (2017, https://doi.org/10.1002/2017GL075071) and Enoto et al. (2017, https://doi.org/10.1038/nature24630).

1. Introduction

1.1. Neutrons as a Footprint of Thunderstorms

The relation between neutron and thunderstorm research has started with the radiocarbon studies of tree rings by Libby and Lukens (1973), as reviewed recently by Rutjes and Ebert (2017). Later Shah et al. (1985) proved a relative increase of neutron emissions over the cosmic background to be correlated with thunderstorms. The first attempts to explain neutron production by lightning focused on fusion, and dominated the literature for some decades, but this mechanism was disproven by Babich and Roussel-Dupré (2007). The fusion mechanism is not possible due to a too low energy and density of deuterium in air. Even for electric fields of 20 to 30 times the conventional breakdown field, the neutron yield from fusion remains small in comparison to the original estimates of Libby and Lukens (1973). Babich and Roussel-Dupré (2007) and in more detail Babich et al. (2010) proved that the correct explanation for the occurrence of neutrons in thunderclouds is the photonuclear reaction of gamma rays in the energy range from 10 to 30 MeV with nitrogen or oxygen nuclei. This photonuclear reaction is due to the so-called Giant Dipole Resonance (GDR) mechanism (Baldwin & Klaiber, 1947; Varlamov et al., 1999). Neutron observations are thus a diagnostic tool on ground for the occurrence of gamma rays with energies between 10 and 30 MeV in a thundercloud, a gamma-ray detector can provide a similar prove but the neutrons will then be a signature of gamma rays not present in the photon spectrum due to photonuclear reactions.

1.2. Neutron Production Through TGFs and Gamma-Ray Glows

The photonuclear reaction mechanism requires a source generating gamma rays with energies above 10 MeV which is the approximate binding energy of neutrons in atmospheric nuclei. More precisely, the binding energies are 10.55 MeV for nitrogen, 15.66 MeV for oxygen, and 9.87 MeV for argon (Dietrich & Berman, 1988). There are two known types of high energy atmospheric phenomena that can produce gamma rays above these thresholds, namely, Terrestrial Gamma-ray Flashes (TGFs) and gamma-ray glows.

TGFs are microsecond-long bursts of photons that were first observed from space (Briggs et al., 2010; Fishman et al., 1994); they can be accompanied by bursts of electron positron pairs (Briggs et al., 2011; Dwyer

et al., 2008), and they correlate with leader propagation. Glows, on the other hand, probably originate from relativistic runaway electron avalanches (RREA) in the field of the thundercloud and last much longer, for minutes; they have been observed on ground (where they are called terrestrial ground enhancements by some authors), from balloons and aircraft (Adachi et al., 2008; Chilingarian et al., 2010, 2011; Eack et al., 1996; McCarthy & Parks, 1985; Torii et al., 2002; Tsuchiya et al., 2007). Terrestrial ground enhancements have been found to be correlated with neutron detection as well (Chilingarian et al., 2017). The different properties of flashes and glows have been related to different physical mechanisms as explained by Dwyer et al. (2012) and Rutjes et al. (2016, 2017). While lightning leaders produce TGFs, lightning is observed to terminate gamma-ray glows (Chilingarian et al., 2015; Kelley et al., 2015; McCarthy & Parks, 1985; Tsuchiya et al., 2013).

1.3. Neutron Emissions From Thunderstorms Measured With Different Detectors

Three main types of neutron detectors have been used by different researchers (Chilingarian et al., 2012; Gurevich et al., 2012; Kozlov et al., 2013; Martin & Alves, 2010; Shyam & Kaushik, 1999; Starodubtsev et al., 2012; Toropov et al., 2013; Tsuchiya et al., 2012): a thermal helium-based detector (^{3}He detector), a boron counter detector (^{10}B detector), and the Neutron Monitor NM-64. A thermal detector is most efficient for particles with energy of the order of 1 eV, a boron-based detector has a peak of efficiency at 2.45 MeV, while a Neutron Monitor NM-64 is focused on higher energies and has a small efficiency below the MeV energy range (reaching 10% for 3 MeV and 2% for 0.5 MeV). Hence, all three detector types operate in very distinct and narrow energy windows, which makes it difficult to analyze the whole spectrum.

Recently, Bowers et al. (2017) measured a burst of neutrons after a lightning strike onto a wind turbine. The neutron detection was followed by a glow of gamma-ray photons which were presumably created by the neutrons themselves. Their detection system consists of three scintillation detectors (SmPl and LgPl, where Pl stands for Plastic scintillator; and NaI(Tl)) and two additional electronics for noise control. The neutrons were detected through capture in LgPl that then releases photons with a characteristic energy of 2.223 MeV. The photons appeared on a millisecond time scale and with the characteristic energy signature of neutron capture, consistent with the TGF afterglow predicted by Rutjes et al. (2017).

Enoto et al. (2017) also have measured the TGF afterglow during their measurements of neutrons and positron beams. They have observed gamma rays with time scale and energy cutoff consistent with the neutron capture process along with their β decay record. Their detectors were based on BGO and NaI scintillation crystals and covered the energy range 0.2–48 MeV. Furthermore, they also found and identified the radioactive decay products of the nuclei that had been created by the photonuclear reaction, that is, isotopes such as ^{13}N.

1.4. Neutron Propagation to Ground

Neutrons interact with air through elastic and inelastic scattering and capture. The dominant process is elastic scattering for most of the relevant energy range below 20 MeV, while capture is the most rare process among the three (Köhn et al., 2017). But scattering only cools the neutrons down, while capture is the only loss process. Capture is the most efficient at low neutron energies. Therefore, the secondary gamma rays formed when a neutron is captured in a nucleus have energies of the order of a few MeV due to the energy released during capture. This is the mechanism of the TGF afterglow predicted by Rutjes et al. (2017), and first measured by Bowers et al. (2017) in a downward directed TGF.

1.5. Earlier Simulations

Neutron emissions have been simulated by Babich et al. (2010), Carlson et al. (2010), and Köhn and Ebert (2015). Babich et al. (2010) conclude that there are 4.3×10^{-3} neutrons produced per photon and that the neutron energy is in the range of 0 to 20 MeV both at production and at sea level altitude. The neutrons diffuse to distances of the order of kilometers from the source axis, when reaching ground.

Carlson et al. (2010) assume a RREA spectrum to simulate an initial photon source and calculate neutron production and detection at sea level. Their results are in general agreement with Babich et al. (2010) concerning energy range and estimated production rate. Both papers predict the neutron pulse to last from the order of microseconds to seconds and conclude that the neutrons are produced along the photon trajectory through the atmosphere rather than from a point-like source, in contrast to Martin and Alves (2010).

Köhn and Ebert (2015) simulate a negative lightning leader at the moment of stepping, where the lightning leader is simulated electrostatically as previously by Moss et al. (2006), Celestin and Pasko (2011), Celestin et al. (2012), and Xu et al. (2012). The accelerated electrons are the source of bremsstrahlung photons that produce neutrons. According to Köhn and Ebert (2015), these neutrons have energies up to 20 MeV at source altitude.

Bowers et al. (2017) perform Monte Carlo simulations of TGFs with GEANT4 (http://geant4.web.cern.ch/) to understand the neutron signature in the LgPl detector. A comparison between the measured 1 – 10 MeV photon spectrum and the GEANT4 simulations shows general agreement in the characteristic energy release on the capture reaction, hence confirming their observations. In their simulations they use an initial photon spectrum produced by a RREA, as parameterized by Dwyer et al. (2012), and they simulate neutron creation and propagation to ground. This ground signature is used as an input to filter the particles that reach the detector. Hence, they can infer the number of TGF gamma rays from the observed count rate in the detector on ground. They notice a longer signal of low energy neutrons in their simulations that is due to neutron thermalization in the ground, and not only in the air.

1.6. Questions and Organization of the Paper

In this paper, we split the relevant gamma-ray energies of 10 to 30 MeV into four intervals of 5 MeV width, so we investigate the energy intervals [10 MeV, 15 MeV], [15 MeV, 20 MeV], [20 MeV, 25 MeV], and [25 MeV, 30 MeV] separately. We assume that each energy interval has a flat spectrum of primary gamma rays and that all rays are directed in the same downward direction. This approach allows us to construct particle distributions for arbitrary gamma-ray sources by superposition, without further hypotheses on the initial energy spectrum.

We analyze position, time, and energy distribution of neutrons and photons on the ground. Our results apply to an arbitrary detection altitude when the integrated air density between source position and detection altitude is the same. Our results can also be applied to an arbitrary source energy spectrum with arbitrary temporal characteristics by superposing the energy intervals with appropriate weights. The simulations showed a second photon pulse that is not directly related to the primary gamma ray, but results from collisions between neutrons and air molecules (Rutjes et al., 2017).

The paper is organized as follows: Section 2 explains method and set-up of the simulations. The simulation results are presented in section 3: the neutron distribution at sea level, the energy spectra of photons and neutrons on ground, and the distribution of arrival times. Our simulation results are further analyzed in section 4. In section 5, we compare our results with previous papers. Finally, we summarize our conclusions in section 6.

2. Method and Setup of the Simulations

2.1. FLUKA

We simulate photons and neutrons in air by Monte Carlo simulation with the software package FLUKA (Ferrari et al., 2005), which has a complete physics list for air in our energy regime (Rutjes et al., 2016). FLUKA and other Monte Carlo simulation codes (GEANT4, EGS5, GRRR, MC-PEPTITA) were compared by Rutjes et al. (2016) where a standard input was used to test the effects of the different approximations and methods of each program on the output. The authors have noticed a general agreement between the programs, but differences due to the straggling effect and due to the implementation of friction were observable. The straggling effect is appropriately implemented in FLUKA.

FLUKA is a general purpose tool to simulate particle interaction with matter; it covers a broad range of energies from a few keV to hundreds of TeV. It was originally developed to simulate hadron cascades, and it is being continuously updated by the CERN team. It can also simulate photonuclear reactions described by the Vector Meson Dominance, Delta Resonance, Quasi-Deuteron, and Giant Dipole Resonance (GDR). It uses also a constantly updated tabulated cross-section set. More information on the implemented cross sections is available online in the manual (http://www.fluka.org/content/manuals/FM.pdf). The program does not provide explicit information on how it transports the particles, however it provides several options for how to detect the particles and how to define the media through which they travel. We implemented a user modified routine to detect the particles.

The photon interactions implemented in FLUKA are (Ferrari et al., 2005) pair production, Compton scattering, photoelectric effect, Rayleigh scattering, photon polarization, photonuclear reactions (GDR, Quasideuteron interactions, Vector Meson Dominance Model), and generation and transport of Cherenkov, scintillation, and transition radiation. Since there is no energy gain in our simulations, the energy of the particles will always be below the initial energy, 10 – 30 MeV in this case.

Because at least 10 MeV are required to liberate neutrons in a photonuclear reaction from nitrogen or oxygen nuclei, the neutrons in our simulation always have energies below 20 MeV. In this energy range, FLUKA trans-

Table 1
Number and Lateral Spreading of the Neutrons at Sea Level as a Function of the Altitude of the Photon Source

Source altitude (km)	Lateral spreading (m)	Neutron number on ground	Neutrons per primary photon	Flux density per primary ($cm^{-2}s^{-1}$)
0.3	291	51777	$(1.294 \pm 0.006) \times 10^{-3}$	0.824×10^{-13}
1.0	396	24913	$(6.23 \pm 0.04) \times 10^{-4}$	0.396×10^{-13}
1.5	417	10666	$(2.67 \pm 0.03) \times 10^{-4}$	0.169×10^{-13}
2.0	427	4666	$(1.17 \pm 0.02) \times 10^{-4}$	0.074×10^{-13}
2.5	445	2018	$(5.1 \pm 0.1) \times 10^{-5}$	0.321×10^{-14}
3.0	408	917	$(2.29 \pm 0.07) \times 10^{-5}$	1.459×10^{-15}
4.0	413	227	$(5.7 \pm 0.4) \times 10^{-6}$	0.361×10^{-15}
5.0	373	81	$(2.0 \pm 0.2) \times 10^{-6}$	1.289×10^{-16}
6.0	347	13	$(3 \pm 1) \times 10^{-7}$	2.069×10^{-17}

Note. For each source altitude, 4×10^7 primary photons were used, with a uniform energy distribution between 10 and 30 MeV. The neutron spreading on ground is defined as the standard deviation from the beam axis. The fourth column contains the neutron number per primary photon, with an error estimated as the root of the neutron number. The last column is the average neutron flux density toward the ground calculated with a reference circular area with 1 km radius and a reference time of 0.5 s.

ports the neutrons with a multigroup algorithm using a cross-section library of 260 groups (Ferrari et al., 2005). The angular probabilities are treated with a Legendre polynomial expansion of the actual scattering distribution. Further details on FLUKA physics can be found in the manual available at the official website (http://www.fluka.org/fluka.php).

We use a low energy cutoff of 10 keV for photons and of 10^{-12} eV for neutrons which are the recommended minimum thresholds in FLUKA.

2.2. Setup of Simulations

For this work, a cylindrical domain from sea level up to 19 km altitude and with a radius of 12 km was adopted. The atmospheric density profile of dry air was simulated by 76 layers of constant density with 250 m of height, consisting of 78.085% N_2, 20.950% O_2, and 0.965% Ar. The atmospheric density in these layers was linearly interpolated from the density of the 1976 U.S. standard atmosphere, defined by the U.S. Committee on Extension to the Standard Atmosphere (Coesa, 1976).

All simulations start with a downward directed beam of 10 million photons distributed within a given energy interval and starting at a given altitude, and we detect photons and neutrons at sea level. We decompose the relevant energy regime into four ranges with a uniform spectrum, these ranges are 10–15, 15–20, 20–25, and 25–30 MeV. The source altitudes range from 300 m to 6 km. At higher source altitudes, too few particles reach sea level. So in total we performed 36 different simulations, namely, for nine different source altitudes and for four different energy ranges.

3. Simulated Photon and Neutron Distributions in Space, Time, and Energy at Sea Level

We have analyzed the photon and neutron distributions in space, time, and energy at sea level as a function of the energy spectrum of the source photons and as a function of the source altitude where we assumed that the photons were emitted within one instantaneous burst in the downward direction. As said above, we divided the neutron relevant energy range from 10 to 30 MeV into four intervals of 5 MeV width. We found that the spatial and temporal distributions of photons and neutrons on ground hardly depend on the energy of the source photons. Only the neutron production rate depends strongly on the photon energy. The results related to the total neutron number that depend on the source spectrum will be discussed in the next section. In the present section we present the spectrum independent distributions, and we sum over the four energy intervals; so effectively we here present results for $4 \cdot 10^7$ source photons uniformly distributed over the energy interval of 10 to 30 MeV.

3.1. Neutron Number and Distribution at Sea Level as a Function of Source Altitude

Table 1 shows the number of neutrons per primary photon at sea level and their spatial spread over the ground as a function of photon source altitude; the spatial spread is measured as the standard deviation from the

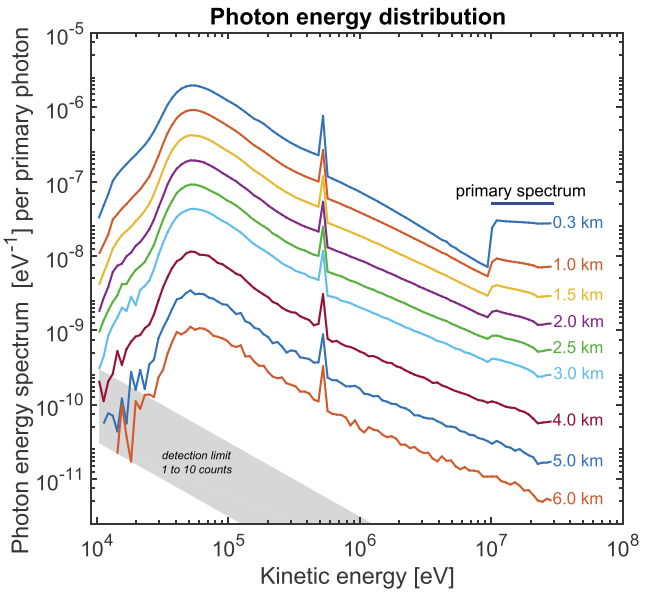

Figure 1. Photon energy spectra at the ground for different source altitudes. The gray shade indicates low statistics.

beam axis. As expected, the neutron number strongly decreases with increasing source altitude. On the otherhand, the spatial spread over the ground is fairly constant with radii ranging from 290 to 450 m. This can be understood based on the spatial distribution of neutron generation and propagation discussed below.

3.2. Energy Spectra of Photons and Neutrons at Sea Level

The energy spectra of photons and neutrons at sea level are presented in Figures 1 and 2 as a function of energy for different source altitudes. The only dependence on the energy spectrum of the source photons lies in the fact that, for example, photons in the energy range from 10 to 15 MeV only produce neutrons with energies below 5 MeV, and hence the spectrum of the produced neutrons has this upper energy limit. However, our simulations show that this initial energy difference of the neutrons rapidly disappears while they cool down through collisions with air molecules. For the neutrons, there are 50 logarithmic bins from 0.1 eV to 20 MeV, while for the photons there are 100 logarithmic bins from 10 keV to 30 MeV, both equally spaced in logarithmic space.

The photon energy spectra recorded at sea level are shown in Figure 1. The source photon spectrum is a uniform distribution between 10 and 30 MeV as indicated in the figure as primary spectrum. This initial spectrum is still clearly visible on ground for source altitudes of 0.3 and 1 km, though attenuated, with a clear discontinuity toward the secondary photon spectrum at lower energies. This discontinuity diminishes for higher source altitudes due to multiple interactions where photons lose energy or disappear, and the discontinuity disappears above 4 km. There is a second discontinuity visible in the spectra at 511 keV which is the positron annihilation line. When photons with energies above 1.02 MeV are available, electron positron pairs can be produced, and the annihilation of the positrons creates the 511 keV line. It can be noticed that the shape of the photon spectrum for longer times and lower energies hardly changes. This is because the distribution is continuously refreshed by higher energy particles losing energy, and hence flowing into the lower energy regimes.

Figure 2 shows the energy spectra of the neutrons. There are two regimes visible: a spectrum with an index of approximately −0.8 for neutron energies up to 10 keV and an exponential cutoff in the MeV energy regime.

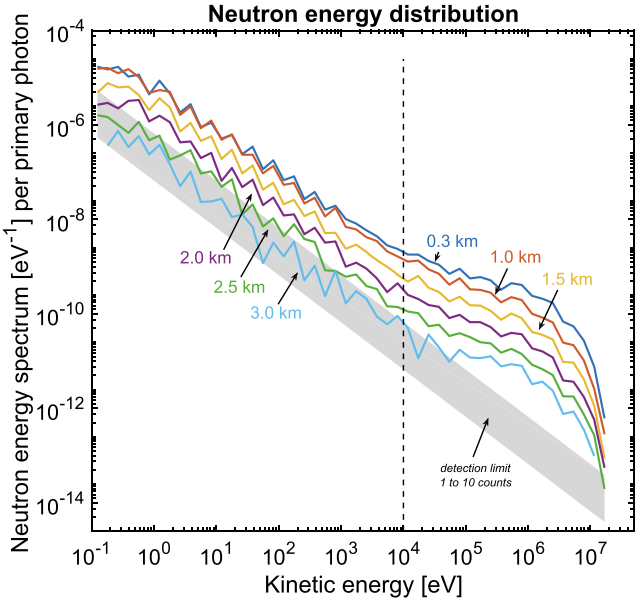

Figure 2. Neutron energy spectra at the ground for different source altitudes. The gray shade indicates low statistics. The vertical line marks the energy range at 10 keV.

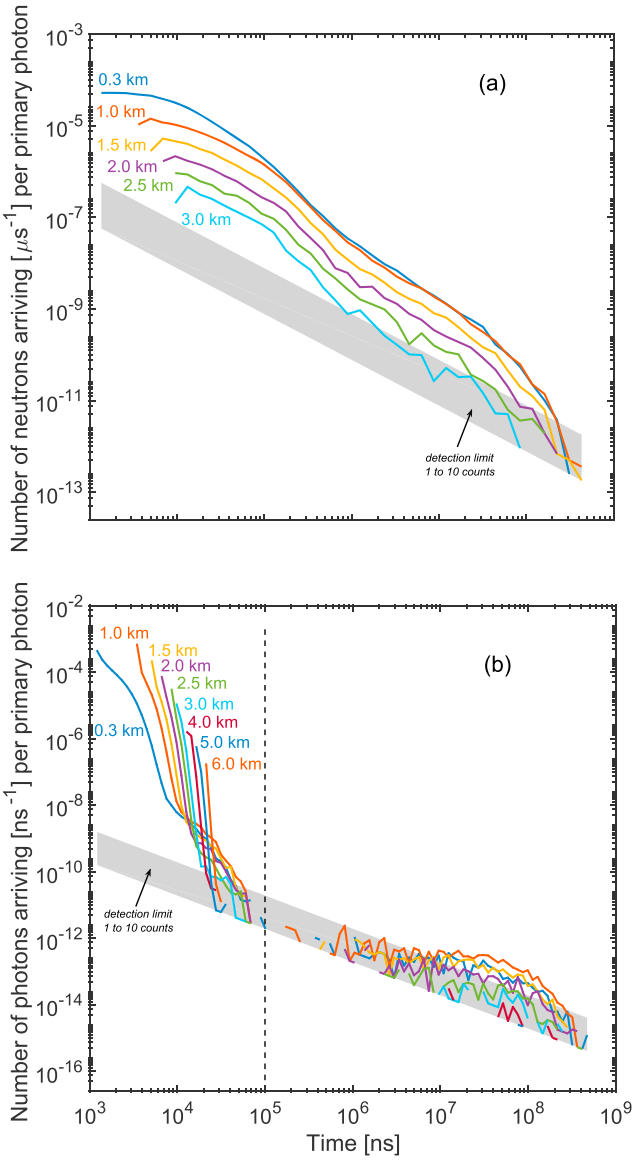

Figure 3. Distribution of arrival times of (a) neutrons and (b) photons on ground per primary. The different source altitudes are indicated by the legend. The vertical line marks the end of the primary photon pulse at 0.1 ms. The gray shade indicates low statistics.

The latter depends on the spectrum of the source photons as this determines the maximal neutron energy. However, the shapes of the neutron spectra on ground hardly depend on the source altitude. This is due totheir actual places of generation and to their dynamics as we will explain further below. The neutron energy spectra below 10 keV become noisy (i.e., they become as low as 1 to 10 counts per bin) with increasing source altitude, indicating that low energy neutrons do not reach the ground and rather thermalize in the air through inelastic scattering or capture. The neutron spectra for source altitudes of 4, 5, and 6 km are very noisy and not shown. Due to the strong absorption for large source altitudes as also visible in Table 1, our simulations would have needed a much larger number of primaries ($\gg 10^7$) to identify the neutron spectrum on ground beyond the statistical noise.

3.3. Distribution of Arrival Times of Photons and Neutrons at Sea Level

We also investigated the arrival times of photons and neutrons at sea level, that is, the number of particles arriving per primary per time as a function of time, again for different photon source altitudes. As before, the distribution of arrival times does not depend on the source spectrum.

The distribution of photon arrival times at sea level is shown in Figure 3b; for all source altitudes this distribution exhibits two distinct pulses. The first pulse has a duration of less than 0.1 ms, it starts at the time a photon needs to travel from the source to the ground in a straight line. The photons arriving somewhat later have undergone some scattering along their path. The second photon pulse lasts up to about 500 ms. It appears when photons create neutrons by a photonuclear reaction, and these neutrons release photons at capture. This is the mechanism that creates a TGF afterglow after a TGF, as predicted by Rutjes et al. (2017).

The distribution of neutron arrival times per primary photon is shown in Figure 3a. The first neutrons reach ground shortly after the first photons. They keep arriving up to times of 500 ms. But while the pulse of secondary photons forms, the neutron number decreases. The late neutrons arrive with lower energies than the fast ones, as will be discussed in more detail later.

3.4. Interpretation of the Simulations and the Shape of the Effective Neutron Source

A photon traveling from a source altitude of 300 m straight down will reach ground within 1 μs (with the speed of light of 3×10^8 m/s). On the other hand, if the most energetic neutron with a kinetic energy of 20 MeV would move straight to the ground without any interaction, it would need 5 μs. But since the first neutrons arrive at ground level already after ≈1 μs as well, as shown in Figure 3a, they must have been created along the photon trajectories near the ground and without many interactions with air particles.

Based on the relevant cross sections of photons and neutrons, the concept illustrated in Figure 4 can be developed for their distribution in space, time, and energy: The photon source is assumed as a point-like instantaneous beam directed downward—from which other sources can be constructed by superposition. This photon beam broadens slightly, while losing energy; the attenuation length is ∼1.5 km (Rutjes et al., 2017) until the photon energy drops below 10 MeV and the photon cannot produce neutrons anymore. The neutrons are created everywhere along the trajectories of the sufficiently energetic photons, therefore the effective neutron source has a cone like structure of about kilometer length. The neutrons initially have energies in the MeV range. They diffuse isotropically while losing energy through collisions. Their attenuation

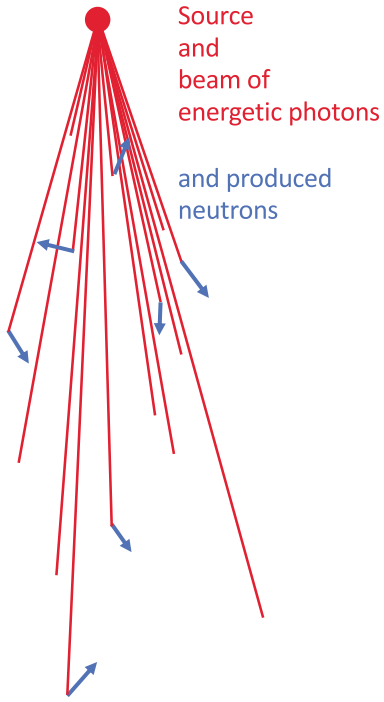

Figure 4. Illustration of the effective neutron source geometry due to a point-like initial photon beam directed downward. The beam of high energy (primary) photons (in red) diverges slightly. Within this beam, individual photons move on straight lines and can create neutrons (in blue) by a photonuclear reaction. The created neutrons diffuse isotropically while they cool down. Photon lines ending without a (blue) neutron have mostly created electron positron pairs; these pairs as well as lower energy photons are not drawn. The spatial dimension is of the order of a kilometer.

length is ~685 m (Köhn et al., 2017). This concept is consistent with the simulated distribution of photons and neutrons in space, time, and energy.

3.5. Second Photon Pulse and Time Dependent Neutron Spectra

All neutrons that do not reach ground will eventually be captured, accompanied with the release of a high energy photon; this is the delayed photon signal visible in Figure 3b. To better identify the relation between spectra and temporal delay, the data of Figures 1–3 are plotted in a different manner in Figure 5: here the spectra of photons and neutrons arriving before or after 0.1 ms are plotted separately.

The majority of the photons arrives within the first photon pulse (before 0.1 ms), while the secondary pulse consists of a relatively small photon number with energy between 10 keV and some MeV, this feature is shown in the upper panels of Figure 5. The ratio of the photon number in the second pulse to the photon number in the first pulse is $\sim 10^{-5}$ for the different source altitudes. This ratio as well as the high energies of the second photon pulse are compatible with the hypothesis that the second photon pulse is created by the capture of neutrons that were created by a photonuclear reaction from the primary photons, see Rutjes et al. (2017) for a further discussion.

The spectra of the neutrons arriving before or after 0.1 ms are shown in the lower panels of Figure 5. The early arriving neutrons have much higher energies which is consistent with the concept that they were created by photons near the ground and have not collided much with air molecules. The neutrons arriving after 0.1 ms have mostly energies below 1 MeV, since they were created earlier when still many energetic photons were available, so they had more time to lose energy through collisions while diffusing through the atmosphere. These numerous and relatively cool *late* neutrons create the second photon pulse discussed above.

4. Neutron Detection on Ground as a Function of Spectrum and Altitude of the Photon Source

We now investigate how the neutron production depends on the spectrum of the photon source.

4.1. Construction of an Arbitrary Photon Source Spectrum

In our simulations, we have divided the photon energy range into four intervals within the energy range relevant for neutron production: 10–15, 15–20, 20–25, 25–30 MeV; these four intervals are labeled as $i = 1, 2, 3, 4$ below. Figure 6 shows the total neutron count per primary as a function of photon source altitude for the four energy intervals of primary photons. Photons within the energy intervals from 20 to 25 MeV and from 25 to 30 MeV create about the same large number of neutrons on ground, and they do this for every source altitude. This is related to the fact that the photonuclear cross-section of nitrogen has a maximum at 23 MeV (Oblozinsky`, 2000). The photon energy range of 10–15 MeV, on the other hand, has the lowest neutron production for all source altitudes.

The number of neutrons $N_i(h)$ on ground per primary photon in one of the four energy intervals $i = 1, 2, 3, 4$ can be approximated as a function of source altitude h as

Table 2
Interpolated Values for the Parameters ℓ_i and I_i in Equation (1) for the Different Energy Ranges of the Source Photons

Label i	Energy Range (MeV)	ℓ_i (m)	I_i per primary
1	10–15	565	1.0×10^{-4}
2	15–20	740	8.3×10^{-4}
3	20–25	667	4.1×10^{-3}
4	25–30	735	2.9×10^{-3}

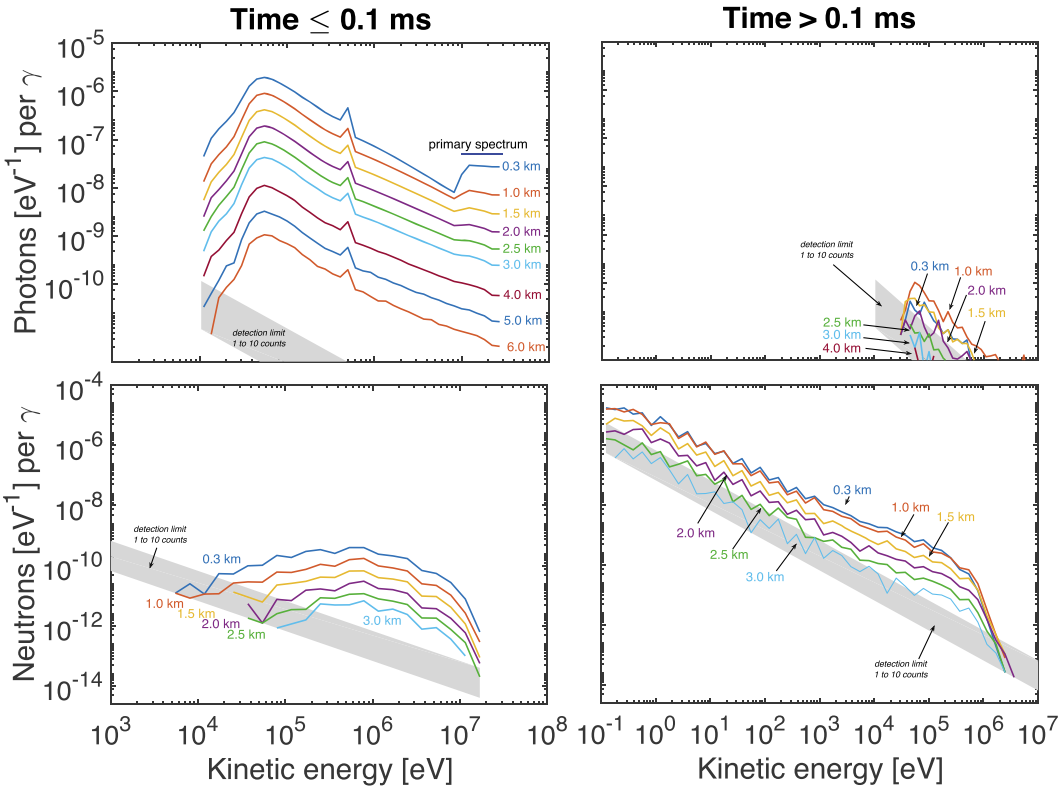

Figure 5. Energy distributions of photons (top row) and neutrons (bottom row) as in Figures 1 and 2, but now differentiated between arriving before 0.1 ms (left column) or after 0.1 ms (right column).

$$N_i(h) = I_i\, e^{-h/\ell_i}, \tag{1}$$

with the values of ℓ_i and I_i given in Table 2. The parameters were determined by interpolating the neutron number for the source altitude h = 300 m and for the highest source altitude with neutron counts for the respective energy interval i. (It should be noted that the exponential ansatz of the equation implicitly assumes a constant air density, therefore it is limited to altitudes below 5 or 6 km. For larger altitudes the variation of air density needs to be taken into account.)

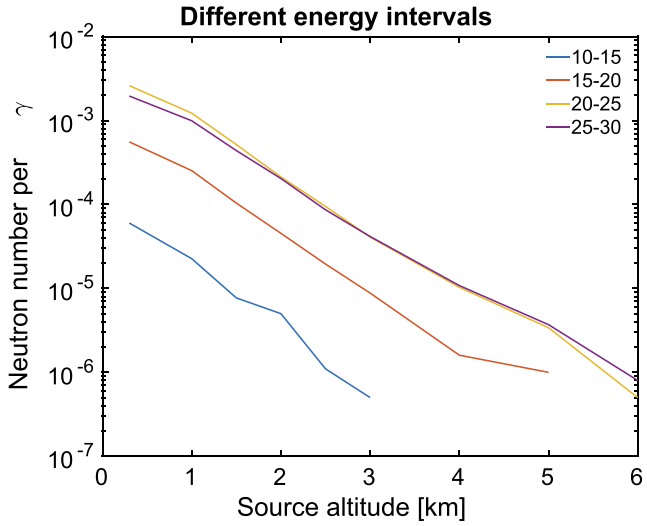

Figure 6. Neutron number on ground per primary photon as a function of source altitude. The lines refer to the four different energy ranges of 10–15, 15–20, 20–25, 25–30 MeV, as indicated in the legend.

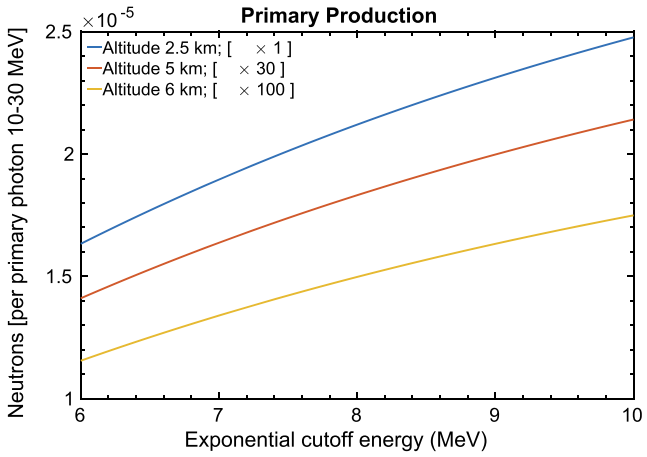

Figure 7. Neutron number per primary at the ground, n_γ, plotted as a function of the source photon spectrum for different source altitudes. The source spectrum is parameterized by an relativistic runaway electron avalanches spectrum (3) with exponential cutoff energy E_{th}. The curves for 5 and 6 km are multiplied by scaling factors of 30 or 100 in order to display all curves in the same plot.

In Table 2, it can be noted, that ℓ_i is not a monotonous function of the gamma-ray energy, and this has a physical reason. As the photonuclear cross section has a maximum at 23 MeV, photons in the energy range of 20 to 25 MeV liberate neutrons closer to the photon source, that is, at a higher altitude. Therefore, these neutrons have a lower probability to reach the ground, because effectively they have to traverse a larger distance. Based on this argument, one would expect ℓ_i to be largest for photons with 10–15 MeV, but then the neutrons have initial energies as low as 0–5 MeV and will not diffuse far before losing their energy.

The neutron number n_γ per primary photon in the energy range of 10–30 MeV for an arbitrary downward directed gamma-ray source with spectrum $f(E)$ at altitude h can now be approximately calculated as

$$n_\gamma \approx \sum_{i=1}^{4} a_i\, N_i(h), \quad a_i = \int_{(5+5i)MeV}^{(10+5i)MeV} f(E)dE \Big/ \int_{10MeV}^{30MeV} f(E)dE, \qquad (2)$$

where a_i is the number of photons in each energy interval i within the distribution $f(E)$.

4.2. Results for Different RREA Spectra and Source Altitudes

The photon spectrum is frequently assumed to be a stationary RREA spectrum (Dwyer et al., 2012) parameterized as

$$f(E) = \frac{1}{E}\, e^{-E/E_{th}}, \qquad (3)$$

with the exponential cutoff E_{th}. The number of photons with energy above the photonuclear reaction threshold increases with E_{th}.

Figure 7 shows the neutron production as a function of this exponential cutoff for source altitudes of 2.5, 5, and 6 km, calculated with equation (2). Two distinct features can be seen: First, for E_{th} varying from 6 to 10 MeV, the neutron detection on ground varies only by a factor of 1.5; this means that the neutron detection is fairly insensitive to this parameter for all source altitudes. On the other hand, the dependence on source altitude is quite strong; this is why we introduced the altitude dependent multiplication factors in the plot to display all curves. The neutron number on ground per primary photon in the right energy range is therefore characteristic for the source altitude.

4.3. Arbitrary Photon Sources and Detection Altitudes

Of course, the neutron number at sea level can be calculated in the same way as above for any other source spectrum and altitude.

If the detection is not at sea level, one has to consider that the results should be the same if the particles had the same probability to collide with air particles; this means that they must have crossed the same air density n integrated from start to end point.

Up to now, we have focused on the products of a single instantaneous point-like photon beam directed downward. Beams with other distributions in space and time can be constructed from it by superposition.

5. Discussion

Carlson et al. (2010) and Babich et al. (2010) have simulated neutron production from specific photon sources and altitudes. Carlson et al. (2010) used a measured TGF photon spectrum parameterized as in equation (3), their results are summarized in Table 3 and can be directly compared to Figure 7. In agreement with

Table 3
Number of Neutrons at Sea Level per Primary by Different Authors

Source altitude (km)	Carlson et al. (2010)	Babich et al. (2010)	Present work
2.5	2.3×10^{-4}	n.a.	2.0×10^{-4}
5.0	6×10^{-6}	2.4×10^{-6}	8.1×10^{-6}

Carlson et al. (2010) and Babich et al. (2010), our results show that the effective neutron source is extended along the photon beam.

Bowers et al. (2017) perform a similar analysis as we do. They simulate neutrons measured on ground that are generated by an instantaneous release of an RREA spectrum of gamma rays moving downward, with $E_{th} = 6.5$ MeV. Source altitudes are 0.5, 1.0, and 1.5 km (for a Japanese winter thunderstorm). But, since they focus in a given spectrum, their work does not provide the possibility of generalization as the present work.

Toropov et al. (2013) have observed that lightning discharges and neutron bursts are well correlated; they registered several discharges, and some were accompanied by neutron burst of approximately 2 min duration. According to the present work, this suggests that there were multiple gamma-ray emissions during a single lightning discharge to generate the neutron pulse detected on ground as the neutron signal from an instantaneous gamma-ray pulse does not last longer than a fraction of a second when it arrives from 3 km altitude or less; for larger altitudes the signal would be very small, as we have calculated.

In our simulations, the vast majority of neutrons are concentrated in an area with less than 1 km radius around the beam axis, as shown in section 3.1; and they arrive within some hundreds of milliseconds, as shown in section 3.3. The average flux density can be calculated with these parameters; it is shown in the last column of Table 1 to allow an estimate whether it can be measured with a given detector.

Martin and Alves (2010) measured a neutron area density of 20 cm^{-2}, but their detector was efficient only in the thermal part of the energy spectrum up to 1 eV; therefore, they missed a great part of the neutron spectrum. They estimated that the initial neutron number was $10^{12} - -10^{13}$ assuming that they came from a point-like source and spread isotropically within a sphere of 1–2 km to their thermal detector.

Other measurements such as the flux of 4×10^{-3} cm^{-2}/s reported by Starodubtsev et al. (2012) took into account only neutrons with energy above 10 MeV. As our results show (Figure 5), neutrons with energy above 10 MeV reach the detection plane within 0.1 ms, so the flux reported by Starodubtsev et al. (2012) may be a result of multiple emissions due the integration time in their measurements.

Considering that the integrated atmospheric density between 0 and 6 km is similar to the value between 6 and 400 km and taking into account that the number of neutron per primary at the ground is of the order of 10^{-7} for a source altitude of 6 km, a larger number of primary photons in the emission would be needed to generate detectable neutrons at the ground and at satellite altitudes. And as the neutrons travel to satellite altitudes, the particles have a lot more space to diffuse than during their motion to the ground, making neutron detection at satellite altitudes very difficult.

Recent TGF measurements (Gjesteland et al., 2015) have shown events that were estimated to have approximately $10^{17} - -10^{20}$ source photons with energy above 1 MeV. The measurements were done in the 25 keV–17 MeV energy range, but the maximum detected energy was 11 MeV. Despite the large quantity of photons with energy above 1 MeV, the neutron binding energy in atmospheric nuclei is at least 10 MeV and the neutron production for 10–15 MeV is small compared to the peak values, as discussed in section 3.2. In order for such events to produce ground detectable neutrons, the source energy must be higher than the detected energy. The energy range must cover at least the peak energy range of photonuclear cross section, that is, 20–25 MeV. Since our results show that although the four energy intervals contribute with similarly shaped spectra and pulses, the absolute number of neutrons is dominated by the energy range 20–30 MeV by at least one order of magnitude, as can be seen in Figure 6.

6. Conclusions and Outlook

We simulated neutron footprints in space and time from gamma-ray point sources with initial photon energy between 10 and 30 MeV; and we differentiated between four initial energy intervals of 5 MeV width. Clearly we see that even if the photons start from a point, neutrons do not originate from a point, but they are produced along the kilometer long paths of the high energy (primary) photons, as illustrated in Figure 4. This fact limits simple inverse approximations on the amount of photons needed to explain observed neutron fluxes. The fluxes provided here can be used for better estimations.

We observed that the neutron spectra for the four different gamma-ray energy intervals do not change significantly, but the number of neutrons produced depends on the gamma-ray energy. In other words, as the number of neutrons produced is so sensitive to the gamma-ray energy, the neutron yield depends on the

initial gamma-ray spectrum. We calculated the number of neutrons as function of the characteristic (mean) energy cutoff of a steady state RREA for several altitudes, see Figure 7. This dependence can be used to calculate the original number of photons, for example, in a gamma-ray glow, when the characteristic (mean) energy cutoff, E_{th} in equation (3), can be approximated based for example on its sensitivity to electric field. Or in the other direction, knowing the total neutron to photon ratio results in the characteristic (mean) energy cutoff (assuming RREA) and by that in a diagnostic for the ambient electric field.

From the energetic and spatiotemporal characteristics of the neutron signal, we conclude that the neutron source is spread in space by photon motion, as illustrated in Figure 4. There are neutrons arriving at sea level at the same time as the photons, indicating that the neutrons were produced at low altitudes so they could coincide with the pulse of primary photons, as shown in Figure 5; and also there are neutrons arriving at sea level after the pulse of photons from the source is gone, meaning that these neutrons were created at high altitudes or collided enough with air particles that their travel time to the ground is much longer. These neutrons have characteristically lower energies. In fact, the arrival times of gamma rays and neutrons after a gamma-ray burst (as presented in Figures 3 and 5) depend in a characteristic manner on the source altitude, and allow its determination.

Since the photons cannot have many interactions without leaving the energy range of photonuclear reaction, we estimate that most neutrons are created on a cone of kilometer length during the photon motion downward; and the neutrons' lateral spreading must be due to their collisions with air molecules. These neutron collisions with air molecules occur on a longer time scale than the time scale of the source particles and generate a second photon pulse constituting the TGF afterglow (Rutjes et al., 2017).

Acknowledgments
G.D. acknowledges funding by CAPES, CNPq, and FAPESP via the grant LEONA 2012/20366-7. C.R. acknowledges funding by FOM Project 12PR3041 that also supported G.D.'s extended visit in The Netherlands. I.S.F. thanks CNPqs grant PDE(234529/2014-08), and also FAPDF grant 0193.000868/2015, 03/2015. F.S.S.T would like to thank FAPESP, the São Paulo Research Foundation for partially supporting this research via the grant LEONA 2012/20366-7. A sample of our FLUKA input may be found in the link: https://gitlab.com/gdiniz/fluka_input_card/blob/master/FLUKA

References

Adachi, T., Takahashi, Y., Ohya, H., Tsuchiya, F., Yamashita, K., Yamamoto, M., & Hashiguchi, H. (2008). Monitoring of lightning activity in Southeast Asia: Scientific objectives and strategies. Kyoto Working Papers on Area Studies: G-COE Series.

Babich, L. P., Bochkov, E. I., Kutsyk, I. M., & Roussel-Dupré, R. A. (2010). Localization of the source of terrestrial neutron bursts detected in thunderstorm atmosphere. *Journal of Geophysical Research*, *115*, A00E28. https://doi.org/10.1029/2009JA014750

Babich, L. P., & Roussel-Dupré, R. A. (2007). Origin of neutron flux increases observed in correlation with lightning. *Journal of Geophysical Research*, *112*, D13303. https://doi.org/10.1029/2006JD008340

Baldwin, G. C., & Klaiber, G. S. (1947). Photo-fission in heavy elements. *Physical Review*, *71*(1), 3–10.

Bowers, G. S., Smith, D. M., Martinez-McKinney, G., Kamogawa, M., Cummer, S., Dwyer, J., et al. (2017). Gamma ray signatures of neutrons from a terrestrial gamma ray flash. *Geophysical Research Letters*, *44*, 10,063–10,070. https://doi.org/10.1002/2017GL075071

Briggs, M. S., Connaughton, V., Wilson-Hodge, C., Preece, R. D., Fishman, G. J., Kippen, R. M., et al. (2011). Electron-positron beams from terrestrial lightning observed with Fermi GBM. *Geophysical Research Letters*, *38*, L02808. https://doi.org/10.1029/2010GL046259

Briggs, M. S., Fishman, G. J., Connaughton, V., Bhat, P. N., Paciesas, W. S., Preece, R. D., et al. (2010). First results on terrestrial gamma ray flashes from the Fermi Gamma-ray Burst Monitor. *Journal of Geophysical Research*, *115*, A07323. https://doi.org/10.1029/2009JA015242

Carlson, B., Lehtinen, N. G., & Inan, U. S. (2010). Neutron production in terrestrial gamma ray flashes. *Journal of Geophysical Research*, *115*, A00E19. https://doi.org/10.1029/2009JA014696

Celestin, S., & Pasko, V. P. (2011). Energy and fluxes of thermal runaway electrons produced by exponential growth of streamers during the stepping of lightning leaders and in transient luminous events. *Journal of Geophysical Research*, *116*, A03315. https://doi.org/10.1029/2010JA016260

Celestin, S., Xu, W., & Pasko, V. P. (2012). Terrestrial gamma ray flashes with energies up to 100 MeV produced by nonequilibrium acceleration of electrons in lightning. *Journal of Geophysical Research*, *117*, A05315. https://doi.org/10.1029/2012JA017535

Chilingarian, A., Bostanjyan, N., & Vanyan, L. (2012). Neutron bursts associated with thunderstorms. *Physical Review D*, *85*(8), 85017. https://doi.org/10.1103/PhysRevD.85.085017

Chilingarian, A., Chilingaryan, S., Karapetyan, T., Kozliner, L., Khanikyants, Y., Hovsepyan, G., et al. (2017). On the initiation of lightning in thunderclouds. *Scientific Reports*, *7*, 1371. https://doi.org/10.1038/s41598-017-01288-0

Chilingarian, A., Daryan, A., Arakelyan, K., Hovhannisyan, A., Mailyan, B., Melkumyan, L., et al. (2010). Ground-based observations of thunderstorm-correlated fluxes of high-energy electrons, gamma rays, and neutrons. *Physical Review D*, *82*(4), 43009. https://doi.org/10.1103/PhysRevD.82.043009

Chilingarian, A., Hovsepyan, G., & Hovhannisyan, A. (2011). Particle bursts from thunderclouds: Natural particle accelerators above our heads. *Physical Review D*, *83*(6), 62001. https://doi.org/10.1103/PhysRevD.83.062001

Chilingarian, A., Hovsepyan, G., Khanikyanc, G., Reymers, A., & Soghomonyan, S. (2015). Lightning origination and thunderstorm ground enhancements terminated by the lightning flash. *Europhysics Letters*, *110*(4), 49001.

Coesa, U. (1976). *Standard atmosphere, 1976*. Washington, DC: US Government Printing Office.

Dietrich, S. S., & Berman, B. L. (1988). Atlas of photoneutron cross sections obtained with monoenergetic photons. *Atomic Data and Nuclear Data Tables*, *38*(2), 199–338.

Dwyer, J. R., Grefenstette, B. W., & Smith, D. M. (2008). High-energy electron beams launched into space by thunderstorms. *Geophysical Research Letters*, *35*, L02815. https://doi.org/10.1029/2007GL032430

Dwyer, J. R., Smith, D. M., & Cummer, S. A. (2012). High-energy atmospheric physics: Terrestrial gamma-ray flashes and related phenomena. *Space Science Review*, *173*, 133–196. https://doi.org/10.1007/s11214-012-9894-0

Eack, K. B., Beasley, W. H., Rust, W. D., Marshall, T. C., & Stolzenburg, M. (1996). Initial results from simultaneous observation of X-rays and electric fields in a thunderstorm. *Journal of Geophysical Research*, *101*(D23), 29,637–29,640. https://doi.org/10.1029/96JD01705

Enoto, T., Wada, Y., Furuta, Y., Nakazawa, K., Yuasa, T., Okuda, K., et al. (2017). Photonuclear reactions triggered by lightning discharge. *Nature*, *551*, 481–484.

Ferrari, A., Sala, P. R., Fasso, A., & Ranft, J. (2005). Fluka: A multi-particle transport code (program version 2005). Tech. rep.
Fishman, G. J., Bhat, P. N., Mallozzi, R., Horack, J. M., Koshut, T., Kouveliotou, C., et al. (1994). Discovery of intense gamma-ray flashes of atmospheric origin. *Science*, *264*, 1313–1316. https://doi.org/10.1126/science.264.5163.1313
Gjesteland, T., Østgaard, N., Laviola, S., Miglietta, M., Arnone, E., Marisaldi, M., et al. (2015). Observation of intrinsically bright terrestrial gamma ray flashes from the Mediterranean basin. *Journal of Geophysical Research: Atmospheres*, *120*, 12,143–12,156. https://doi.org/10.1002/2015JD023704
Gurevich, A., Antonova, V., Chubenko, A., Karashtin, A., Mitko, G., Ptitsyn, M., et al. (2012). Strong flux of low-energy neutrons produced by thunderstorms. *Physical Review Letters*, *108*(12), 125001. https://doi.org/10.1103/PhysRevLett.108.125001
Kelley, N. A., Smith, D. M., Dwyer, J. R., Splitt, M., Lazarus, S., Martinez-McKinney, F., et al. (2015). Relativistic electron avalanches as a thunderstorm discharge competing with lightning. *Nature Communications*, *6*, 7845.
Köhn, C., Diniz, G., & Harakeh, M. N. (2017). Production mechanisms of leptons, photons, and hadrons and their possible feedback close to lightning leaders. *Journal of Geophysical Research: Atmospheres*, *122*, 1365–1383. https://doi.org/10.1002/2016JD025445
Köhn, C., & Ebert, U. (2015). Calculation of beams of positrons, neutrons, and protons associated with terrestrial gamma ray flashes. *Journal of Geophysical Research: Atmospheres*, *120*, 1620–1635. https://doi.org/10.1002/2014JD022229
Kozlov, V., Mullayarov, V., Starodubtsev, S., & Toropov, A. (2013). Neutron bursts during cloud-to-ground discharges of lightning. *Bulletin of the Russian Academy of Sciences: Physics*, *77*(5), 584–586.
Libby, L. M., & Lukens, H. R. (1973). Production of radiocarbon in tree rings by lightning bolts. *Journal of Geophysical Research*, *78*(26), 5902–5903. https://doi.org/10.1029/JB078i026p05902
Martin, I. M., & Alves, M. A. (2010). Observation of a possible neutron burst associated with a lightning discharge? *Journal of Geophysical Research*, *115*, A00E11. https://doi.org/10.1029/2009JA014498
McCarthy, M., & Parks, G. (1985). Further observations of X-rays inside thunderstorms. *Geophysical Research Letters*, *12*(6), 393–396. https://doi.org/10.1029/GL012i006p00393
Moss, G. D., Pasko, V. P., Liu, N., & Veronis, G. (2006). Monte Carlo model for analysis of thermal runaway electrons in streamer tips in transient luminous events and streamer zones of lightning leaders. *Journal of Geophysical Research*, *111*, A02307. https://doi.org/10.1029/2005JA011350
Oblozinsky`, P. (2000). Handbook of photonuclear data for applications: Cross sections and spectra. International Atomic Energy Association Report IAEA-TECDOC-1178, Vienna, Austria.
Rutjes, C., Diniz, G., Ferreira, I. S., & Ebert, U. (2017). TGF afterglows: A new radiation mechanism from thunderstorms. *Geophysical Research Letters*, *44*, 10,702–10,712. https://doi.org/10.1002/2017GL075552
Rutjes, C., & Ebert, U. (2017). A natural neutron source. *Physics World*, *October 2017*, 13–15.
Rutjes, C., Sarria, D., Skeltved, A. B., Luque, A., Diniz, G., Østgaard, N., & Ebert (2016). Evaluation of Monte Carlo tools for high energy atmospheric physics. *Geoscientific Model Development*, *9*(11), 3961–3974. https://doi.org/10.5194/gmd-9-3961-2016
Shah, G., Razdan, H., Bhat, C., & Ali, Q. (1985). Neutron generation in lightning bolts. *Nature*, *313*, 773–775. https://doi.org/10.1038/313773a0
Shyam, A., & Kaushik, T. (1999). Observation of neutron bursts associated with atmospheric lightning discharge. *Journal of Geophysical Research*, *104*(A4), 6867–6869. https://doi.org/10.1029/98JA02683
Starodubtsev, S. A., Kozlov, V., Toropov, A., Mullayarov, V., Grigor'ev, V. G., & Moiseev, A. (2012). First experimental observations of neutron bursts under thunderstorm clouds near sea level. *Soviet Journal of Experimental and Theoretical Physics Letters*, *96*(3), 188–191. https://doi.org/10.1134/S0021364012150106
Torii, T., Takeishi, M., & Hosono, T. (2002). Observation of gamma-ray dose increase associated with winter thunderstorm and lightning activity. *Journal of Geophysical Research*, *107*(D17), 4324. https://doi.org/10.1029/2001JD000938
Toropov, A., Kozlov, V., Mullayarov, V., & Starodubtsev, S. (2013). Experimental observations of strengthening the neutron flux during negative lightning discharges of thunderclouds with tripolar configuration. *Journal of Atmospheric and Solar-Terrestrial Physics*, *94*, 13–18.
Tsuchiya, H., Enoto, T., Iwata, K., Yamada, S., Yuasa, T., Kitaguchi, T., et al. (2013). Hardening and termination of long-duration γ rays detected prior to lightning. *Physical Review Letters*, *111*, 15001. https://doi.org/10.1103/PhysRevLett.111.015001
Tsuchiya, H., Enoto, T., Yamada, S., Yuasa, T., Kawaharada, M., Kitaguchi, T., et al. (2007). Detection of high-energy gamma rays from winter thunderclouds. *Physical Review Letters*, *99*(16), 165002. https://doi.org/10.1103/PhysRevLett.99.165002
Tsuchiya, H., Hibino, K., Kawata, K., Hotta, N., Tateyama, N., Ohnishi, M., et al. (2012). Observation of thundercloud-related gamma rays and neutrons in Tibet. *Physical Review D*, *85*(9), 92006. https://doi.org/10.1103/PhysRevD.85.092006
Varlamov, A., Varlamov, V., Rudenko, D., & Stepanov, M. (1999). Atlas of giant dipole resonances. Parameters and Graphs of Photonuclear Reaction Cross Sections. INDC (NDS)-394 (pp. 1–311) IAEA NDS, Vienna, Austria.
Xu, W., Celestin, S., & Pasko, V. P. (2012). Source altitudes of terrestrial gamma-ray flashes produced by lightning leaders. *Geophysical Research Letters*, *39*, L08801. https://doi.org/10.1029/2012GL051351